Effect of Cooling Condition on Deformation of Continuously Cast Stainless Steel 304

Tae-Woo Kim and Hwasoo Park

(Submitted 30 May 2003)

This work investigated the effect of the cooling condition on the deformation that was found for continuously cast stainless steel 304 slabs. The transient heat-transfer finite element analysis under various cooling conditions yielded temperature distributions within the slab, which were then used for subsequent calculations of the deformed shape. The asymmetric cooling condition in a cooling pit induced non-uniform and asymmetric thermal gradients with elapsed time. The non-zero final deflection and the reversal of curvature for the slab during cooling were attributed to the combined effect of asymmetric temperature profile and inelastic material property. Parametric studies revealed that a slab material of a low thermal conductivity or yield strength resulted in an increase for final deflection. The present analysis explained the physical cause of the deformation reasonably well.

Keywords casting, finite element analysis, metal processing, stainless steel

1. Introduction

Stainless steels[1] are used in parts requiring corrosion resistance, high resistance to temperature, and formability. In addition, 100% recyclable and aesthetic appealing stainless steel has been a preferred choice of material for architects. Alterations in chemical or thermal process to the base stainless steel (Fe-Cr-Ni) can modify the microstructure and properties of the stainless steel family of alloys. Thus different numbers, which are selected depending on specific applications, are assigned to various stainless steels. The components made with stainless steel, for example, are automobile exhaustive systems (409), body frames (duplex), medical/biomaterials (316), nuclear plants (309, 316), chemical plants (304, 316), as well as household utensils (304, 430). Stainless steel 304 is austenitic with relatively high chromium content. Therefore, the material is particularly suited for parts requiring good corrosion resistance.

Continuous casting[2] has been used to produce nearly all ferrous steels as well as non-ferrous metals due to the high productivity of the technique. Continuous-casting technique have been researched extensively to eliminate material defects,[3] and thereby to produce good quality slabs. Micro-scale defects involve entrapped inclusions, blowholes, pores, and segregations. On the other hand, macro-scale defects can be undesirable process-related deformations or surface/subsurface cracks within slabs. Research reported to date in relation to casting or stainless steel includes fluid flow,[4] microstructure and properties,[5] and thermo-mechanical treatments.[6]

Tae-Woo Kim, School of Mechanical Engineering, Kook-Min University, Seoul, 136-702, Korea; and **Hwasoo Park,** School of Advanced Materials Engineering, Kook-Min University, Seoul, 136-702, Korea. Contact e-mail: twkim@kookmin.ac.kr.

The current study is aimed at understanding the physical phenomenon observed at POSCO (Pohang Iron and Steel Co., Ltd., Pohang, Korea). The continuously cast slabs experienced cooling after complete solidification and cutting. To expedite the cooling process, slabs could be plunged into a water-cooling pit, where the slabs experienced severe cooling rates for some duration. Then the slabs were withdrawn from the cooling pit for further cooling in air until subsequent thermo-mechanical treatment could be provided. The slabs, which were initially flat (* in Fig. 1) before being submerged into the cooling pit, were observed bent (** in Fig. 1 and 2) when they were seen either inside, or immediately after being yanked out of the cooling pit. The curved slab was observed to retain the self-similar deflected shape with minor change in radius of curvature during subsequent cooling. Sometimes, however, the bent shape of the slab had changed significantly during the cooling process, which resulted in curvature reversal from one sign to the opposite sign (*** in Fig. 1 and 2). Curved slabs were undesirable because they tended to be caught and stuck between rollers while in translating motion. Additionally, too large a curvature hampered the subsequent rolling processes, which were designed for flat slabs. The curvature equivalent to maximum deflection in the order of several tens of millimeters could be considered a potential failure. In order to control the undesired deformation, the cause of the deformation that was dependent on the cooling condition needs to be understood.

Information about residual stress within materials is important because the presence of internal stress could cause unexpected distortion or cracking during subsequent thermo-mechanical loading. Residual stress is known to develop within materials by plastic deformation,[7] oxidation,[8] thermal expansion mismatch with uniform cooling,[9] or with non-uniform temperature profiles.[10] The non-uniform temperature profile can be persistent for continuous thermal contact, but it is temporary during rapid cooling or heating. Because temperature distributions were time-dependent, the slabs showed time-dependent deformations. If the slab material deformed beyond the elastic limit, the slab may not return to the original shape even after all external loadings were eliminated. Therefore, a thorough study through deformation and stress analysis is im-

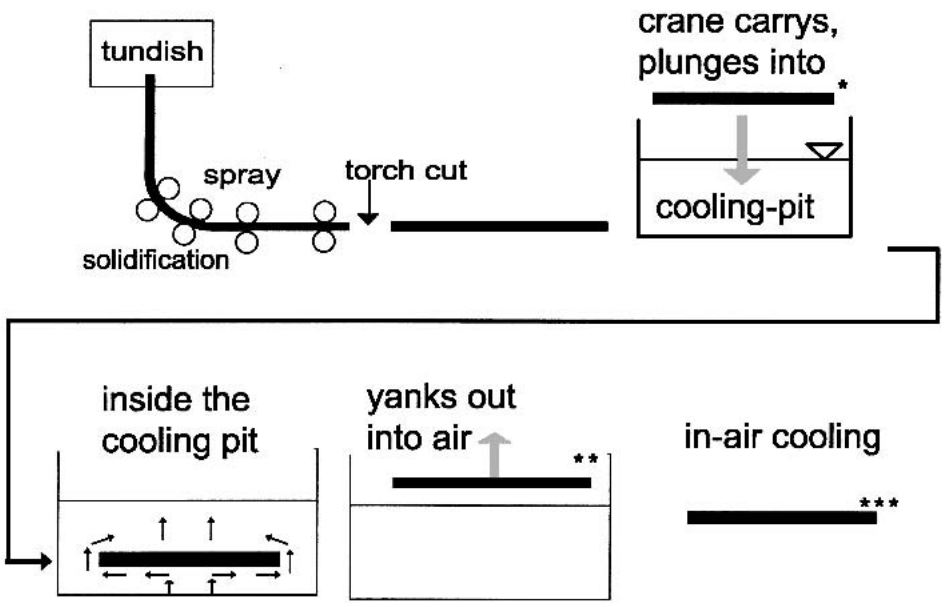

Fig. 1 Schematic diagram of continuous casting and cooling process

portant in explaining the cause of the deformation and in predicting potential failure of the slab.

The present work investigated the effect of the cooling condition on the deformation that was found for continuously cast stainless steel 304 slabs. The finite element model was established on the basis of the actual geometry and the properties of the material. The heat-transfer analysis and the ensuing deformation analysis were performed with changes in cooling condition. The purpose of the present investigation was to elucidate the nature of time-dependent deformation for the slab. The analysis, therefore, were focused on the quantitative estimation of deflection with parametric studies on cooling condition and material properties.

2. Modeling and Analysis Procedure

Dimensions of the slab under simulation were chosen to be 7000 × 200 × 1000 mm (length x depth x width). However, the analysis methodology presented in this investigation can be applied to a slab of different material or changed dimension by slightly modifying finite element modeling. The bent plate was assumed to remain geometrically stable. Due to the symmetry of the problem in width direction, plane-strain analysis was performed for the central longitudinal area. Refined meshes were used toward all surfaces within the slab, because regions near surfaces were expected to experience relatively high thermal gradient. Despite the presence of a half geometric symmetry in the length direction, modeling was made for the full length. This was done because the full modeling could provide a clearer graphic representation of the deflected shape of an entire slab.

Continuously cast solid slabs were spray-cooled on rolls, and were torch-cut into the predetermined length. Some temperature gradient might exist within the slab because the front end of the slab in the length direction underwent solidifying and spray cooling earlier compared with the tail part of the slab. The as-cut slabs were allowed to cool in ambient air for several minutes. During this period of air-cooling, the temperature gradient in the length direction was expected to decrease gradually leading to rather uniform temperature within the slab. Actual temperatures were measured at several locations on the surface of the slab by a radiation pyrometer. It was done just before the slab was plunged into the cooling pit. The initial temperature of the slab was assumed to be the measured average of 700 °C uniform throughout the slab. However, to use more accurate initial temperature distributions, results based on a series of calculations in fluid flow, heat transfer, and solidification processes[11,12] could be used. The crane carried the slab into the water cooling pit until the slab was laid flat on supporting blocks.

When a hot surface is in contact with a pool of coolant liquid, the heat transfer situation is termed "pool boiling."[13] For a large temperature difference between the liquid and the solid surface, the heated liquid at the surface is known to generate bubbles, which grow and break away from the surface with heat removal. In this way, the contact of water in the cooling pit with top surface of the slab would be cooled as the heated water tended to rise upward. The upward motion was developed because the density of the bubble or heated water was to decrease with an increase of the temperature. The cooling water at top surface swept the heat away from the top surface directly, and tended to rise up toward the top free surface of the cooling pit. The detachment of the bubble then gave way for new coolant to flow inward[13] onto the top of the slab.

However, the heated water under the bottom surface of the slab would not directly rise up toward the top free surface level of the cooling pit. This is because the large surface area of the bottom slab blocked the heated water to readily rise up vertically. Instead, the heated water under the bottom surface of the slab tended to go around the sides of the slab (Fig. 1). In

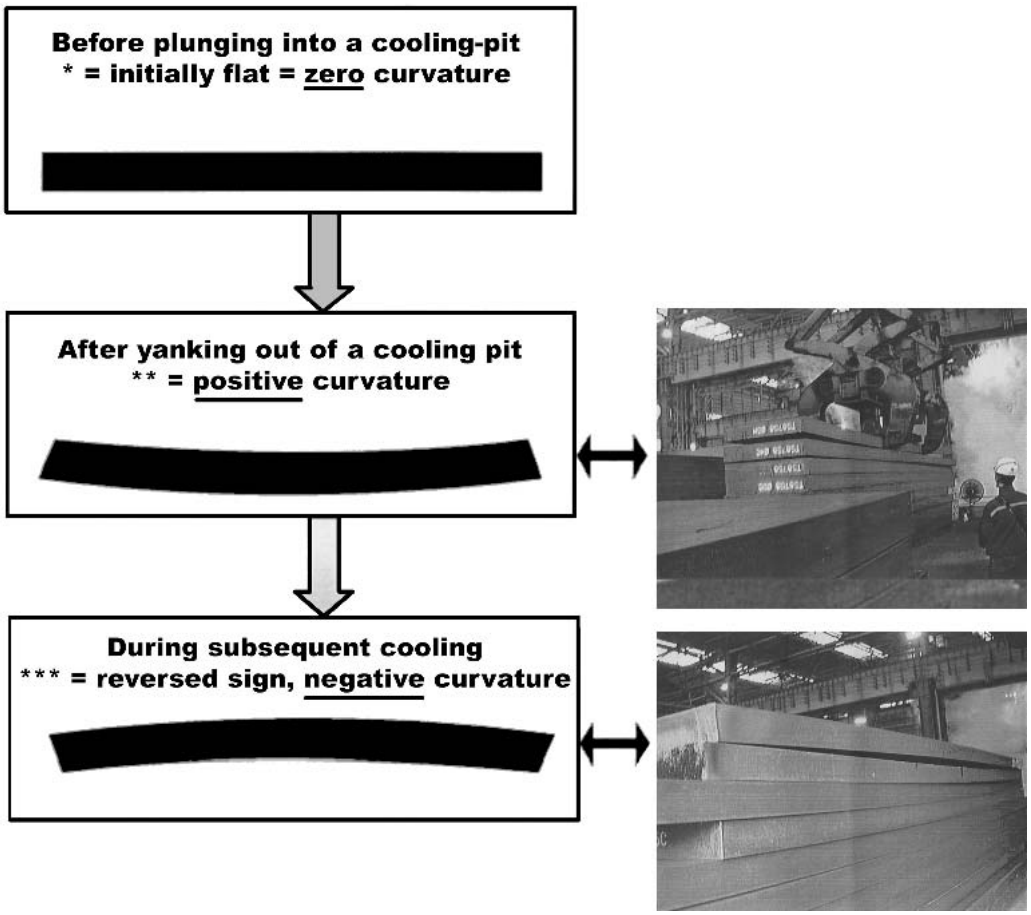

Fig. 2 Typical time-dependent deformations found for stainless steel 304 slab

addition, the vapor at the bottom surface tended to form a vapor blanket at the surface, resulting in a slow down in heat removal process. Consequently, the top surface of the slab was cooled more efficiently compared with the bottom surface, and the bottom surface experienced time-lagged cooling. Thus, the temperature at bottom surface of the slab was expected to be higher than that at top surface at a given time. This cooling difference caused an asymmetric thermal gradient within the slab.

In the current study, the surface heat transfer coefficient, which was assumed to represent the combined effect[14] of convection and radiation at the surface, was chosen. The cooling effect caused by surface radiation was presumed to be smaller than that by convection, and the radiation effect could be similar at the top and bottom surfaces. Thus, the difference in convection coefficient makes the cooling condition distinct at the top and bottom surfaces. The asymmetric cooling difference was modeled by applying different surface heat-transfer coefficients at the top and bottom surfaces. Assuming a temperature-independent heat transfer coefficient is a common practice in simulating quenching process for metals.[15]

The heat flow through external surfaces could vary depending on the severity of the cooling. Estimating the exact heat flow rate out of the slab inside the cooling pit was difficult. The one-dimensional heat transfer equation and boundary conditions, when modeled with surface convection with concomitant conduction, are given by[13]:

$$\frac{\partial^2 T}{\partial y^2} = \frac{1}{D}\left(\frac{\partial T}{\partial t}\right) \quad \text{(Eq 1)}$$

$$h_1[T(L,t) - T_{\text{coolant}}] = -k\frac{\partial T}{\partial y}\Big|_{y=L} \quad \text{(Eq 2a)}$$

$$h_2[T_{\text{coolant}} - T(-L,t)] = -k\frac{\partial T}{\partial y}\Big|_{y=-L} \quad \text{(Eq 2b)}$$

where *T, D, t, h, L* are temperature, thermal diffusivity, time, and surface heat transfer coefficients, and half of the depth, respectively. The origin of *y*-direction is located at the geometric center, and "y" measures the distance in the thickness direction as positive upward.

The surface transfer coefficient during quenching of metals has been reported to be in the order of a thousand.[15,16] In the current study, the coefficient at the top (h_1) was assumed to be a constant of 1000 W/m^{2}K, while the supposedly lower coefficient at the bottom (h_2) was selected between 0 and 1000 W/m^{2}K. The coefficient at left and right sides were assumed to be the same with that at top surface. To better understand the cause of the deformation behavior, temperature distribution

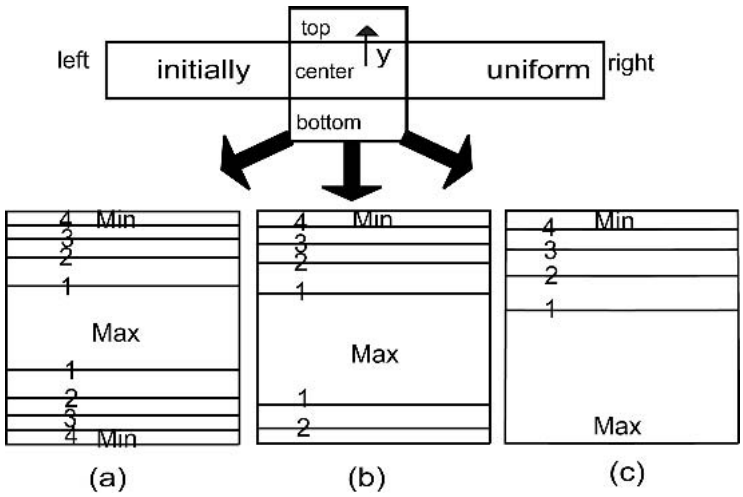

Fig. 3 Three different types of temperature contours with maximum temperature: **(a)** at center; **(b)** between center and bottom; and **(c)** at bottom

under a perfectly symmetric cooling condition was also computed and compared with results obtained under asymmetric cooling conditions.

The calculated temperature distributions as a function of the transient time were inputted for subsequent deformation analysis. Within perfectly elastic range, the total strain (ε) is the sum of the elastic strain and the thermal strain.

$$\varepsilon = \varepsilon_{el} + \varepsilon_{th} = \frac{\sigma}{E} + \alpha \cdot \Delta T \quad \text{(Eq 3)}$$

$$\sigma = E(\varepsilon - \alpha \cdot \Delta T) \quad \text{(Eq 4)}$$

where α and ΔT are the coefficient of thermal expansion and change in temperature, respectively. With the presence of curvature, the strain (ε) within the beam is generally defined as[17]:

$$\varepsilon = \varepsilon_0 - \kappa \cdot y \quad \text{(Eq 5)}$$

$$\kappa = \frac{1}{R} = \frac{M}{EI} = \frac{d^2v}{dx^2} \quad \text{(Eq 6)}$$

where κ, R, and ε_0 are curvature, radius of curvature, and normal strain at neutral axis (i.e., $y = 0$), and *M, EI,* and *v* are bending moment, bending stiffness, and deflection, respectively. The positive direction in *y*-coordinate is shown in Fig. 3. According to the sign convention for the positive moment, the curvature is considered to be positive with concave upwards (sagging downward), and negative with concave downwards (bulging upward).[17] Therefore, stress is given by:

$$\sigma = E(\varepsilon_0 - \kappa \cdot y - \alpha \cdot \Delta T) \quad \text{(Eq 7)}$$

If the deformation exceeds the elastic range, then the permanent plastic strain is summed additionally.

$$\varepsilon = \varepsilon_{el} + \varepsilon_{th} + \varepsilon_{pl} \quad \text{(Eq 8)}$$

Selected thermo-mechanical material properties used for the analysis are shown in Table 1.[18] The stainless steel was modeled to be isotropic, rate-independent, and elastic/perfectly plastic. Because uniform temperature was assumed throughout the slab, the slab was assumed to be flat and stress-free initially. The initial temperature was well below the melting temperature of the stainless steel, thus creep deformation was not considered. Both heat-transfer and subsequent static analysis were performed by commercial finite element program of ABAQUS.[19] 4-node bilinear elements were used.

3. Results and Discussion

Figure 3(a) shows typical transient temperature contours under a perfectly symmetric cooling condition for the slab. The contour numbers (1 through 4) represent different levels of temperature. Number 1 stands for relatively the highest temperature contour line for each case. The temperature contours were symmetric with respect to the neutral axis of the slab. Temperature was maximum at center and uniform along the length direction, which indicated that the temperature gradient was mainly in the thickness direction of the slab except corner regions near left and right sides of the slab. Under asymmetric cooling condition when the top surface cooled faster than the bottom surface, asymmetric temperature distribution was expected in the thickness direction. Two distinct types of asymmetric conditions could be obtained depending on the region for the maximum temperature. Figure 3(b) shows for temperature profile with the maximum temperature developed at a region between center and bottom, compared with Fig. 3(c) with the maximum occurred at bottom. The minimum temperature invariably occurred at top surface.

For a symmetric and three different levels of asymmetric cooling conditions, temperature histories and temperature differences were compared in Fig. 4. The temperature difference, which was initially zero within the slab, increased monotonically until the maximum peak difference was attained, which was followed by a decrease as temperatures within the slab

Table 1 Selected Material Properties of Stainless Steel 304

Property	Value
Specific heat (J/kgK)	500
Density (kg/m^3)	8000
Thermal conductivity (W/mK)	21
Coefficient of thermal expansion (1/°C)	18
Elastic modulus (GPa)	200
Poisson's ratio	0.3
Yield strength (MPa)	410

approached that of the cooling medium. Figure. 4(a)-(d) show that the peak temperature difference between center and top ($=T_{cen}-T_{top}$) changed marginally with the change in heat-transfer coefficient at bottom (h_2). Meanwhile, the peak of the temperature difference between the bottom and top ($=T_{bot}-T_{top}$) increased when h_2 alone was reduced under a fixed value of h_1.

Under symmetric cooling condition (i.e., $h_1 = h_2$), the temperature at bottom was identical to that at top. The maximum temperature occurred always at the center (Fig. 3a and 4a). If the coefficient at bottom (h_2) was selected to be 80% of h_1, the maximum temperature occurred at a region between center and bottom. The temperature at center was always higher than that at bottom (Fig. 3b and 4b). As h_2 was selected to be 5% of h_1, the temperature at center was computed to be higher than that at bottom during initial cooling. But, an overturn of the temperature at bottom over center was obtained after about 500 s, as shown with an arrow in Fig. 4(c). Then, the bottom temperature was higher than that at center during the remaining cooling period. The non-dimensional Biot modulus indicates "the internal thermal resistance" divided by "the external thermal resistance."[20] The Biot modulus is the ratio of heat transfer in to heat conduction away from a surface, and the modulus is proportional to the surface heat transfer coefficient (h) under a constant thermal conductivity (k). When h_2 was set to 0% of h_1, the Biot modulus at bottom became significantly smaller than that at top, indicating high thermal resistance at bottom surface. Therefore, the heat loss at bottom through convection became so limited as compared with heat flow at center toward the top surface through conduction. As a result, the maximum temperature always occurred at bottom (Fig. 3c and 4d).

Figure 5 shows typical time-dependent changes in temperature difference, the deflection at center, and equivalent plastic strain within the same time frame. The minus sign of the deflection (between A and D in Fig. 5) stands for the downward deflection at the geometric center, which results in positive curvature for the slab. Meanwhile, the plus sign (after D in Fig. 5) indicates upward displacement at center implying bulging upwards. Curvature reversal occurs at point D, where the sign of the deflection at the center started to switch from minus to plus. While the temperature difference was increased, the relatively cooler top kept contracting more than the hotter bottom. Due to this mismatch in contraction at top and bottom, the absolute value of downward deflection at center increased until the peak temperature difference was attained. As the temperature difference began to diminish (after C in Fig. 5), the bent slab tended to return to a flat shape and became less curvy. However, if the local temperature gradients were too steep during the initial stage of cooling, then the local region would generate high strain gradient thus plastic strain. The plastic strain began to develop beyond the elastic limit. Because the thermal gradient at bottom was less than that at top, the plastic strain at bottom was computed to be smaller, and began to develop later (at B' in Fig. 5) than that at top (at B in Fig. 5). The accumulated plastic strain at local area prevented the slab from returning to original flatness.

Figure 6 shows typical changes in the deformed shape and the longitudinal stress at top, center, and bottom locations for four different combinations of cooling condition and material behavior. Rapid cooling, often called quenching or thermal shock, induces relatively lower temperature at surface compared with that at center. The lower temperature at surface is known to generate tensile residual stress at surface, which is known to be responsible for surface cracking of brittle materials during rapid cooling.[21] The combination of symmetric cooling condition and elastic behavior lead to tensile and equal residual stress at top and bottom surfaces, which vanished upon the completion of cooling (Fig. 6a). The asymmetric cooling induced downward deflection temporarily, but the elastic behavior generated neither permanent residual stress nor any significant deflection at final state (Fig. 6b). The notion of negligible final residual stress was not true for a slab experiencing elastic–plastic behavior. The residual stress began to develop in tensile (i.e., positive) at surface during the initial stage of cooling, which reversed sign leading to compressive (i.e., negative) residual stress. Under symmetric cooling with elastic–plastic behavior, the residual stress contour remained symmetric with respect to the neutral axis (Fig. 6c). Under asymmetric cooling condition and elastic–plastic behavior, the residual stress state was asymmetric (Fig. 6d). The asymmetric stress indicated unequal contraction at top and bottom, implying the presence of curvature for the slab. Therefore, only when asymmetric temperatures within the slab were combined with yield strength, which is low enough to produce plastic behavior, could non-zero final deflection and the reversal of the curvature for the slab during cooling occur.

A parametric study was made with changes in material property. Figure 7 shows change in time-dependent deflection depending on the yield strength of the slab material. As the yield strength was increased, the final deflection of the slab was reduced approaching zero. It indicates that the slab of significantly high yield strength, which approaches an elastic case, would produce zero deflection indicating a perfect recovery to original configuration for the slab. The slab of larger yield strength generated smaller plastic strain, resulting in smaller final deflection. The largest downward (i.e., negative) deflection for the plastically deformed (hollow symbols in Fig. 7) beam was less negative than that for an elastically deflected (solid square, ■) beam. The difference, which was indicated by an arrow in Fig. 7, resulted in the upward deflection accompanying a curvature reversal during the remaining cooling period.

When a flat beam is bent by purely mechanical bending moment beyond the yield point of the material followed by elastic unloading, the beam tends to regain original flatness. At the time of complete unloading, a permanent residual stress and deflection are known to remain within the beam.[22] During an application of a positive bending moment and subsequent un-

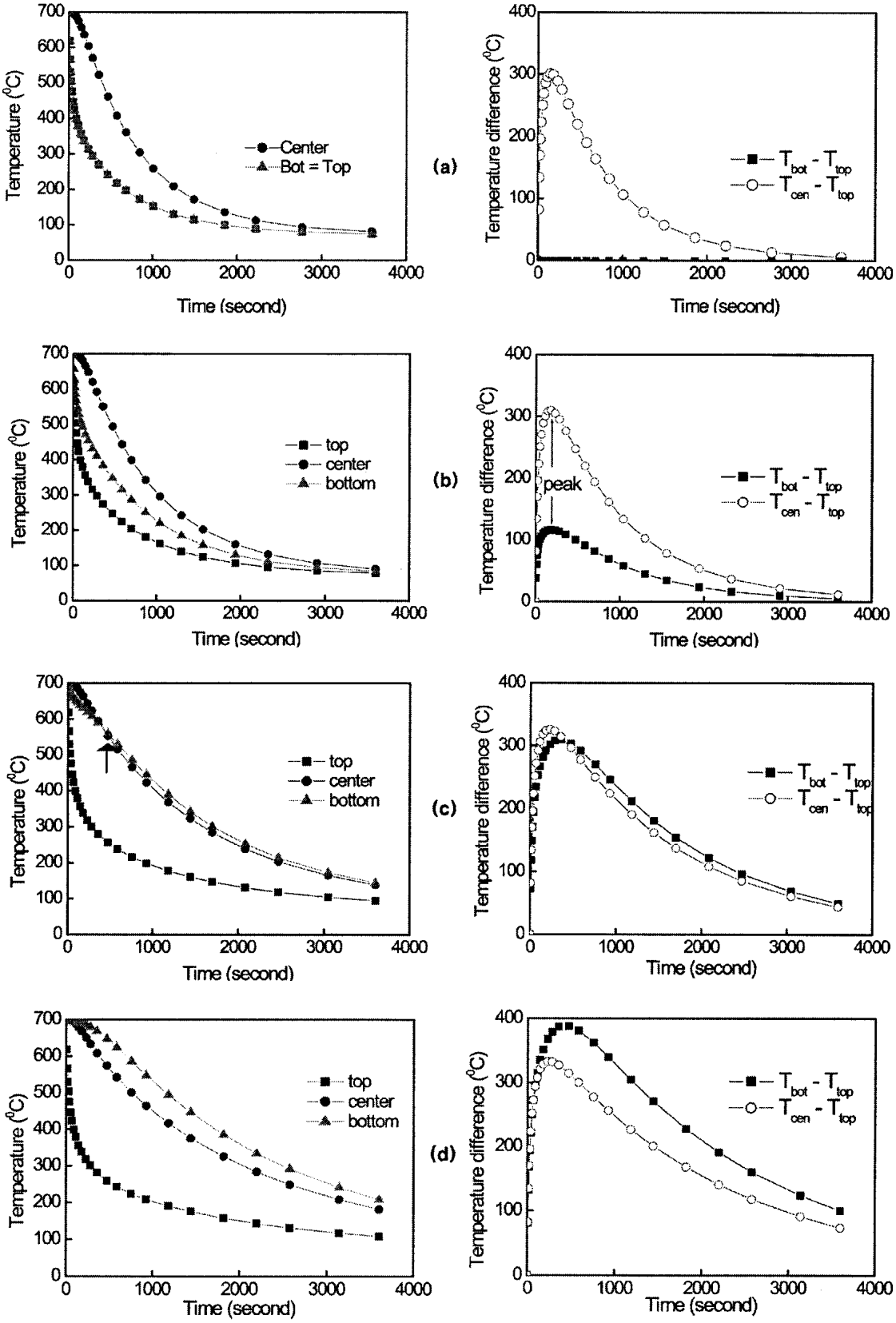

Fig. 4 Temperature and difference with time under four different cooling conditions for the coefficient h_2 equal to: **(a)** 1000; **(b)** 800; **(c)** 50; and **(d)** 0 W/m^{2}K

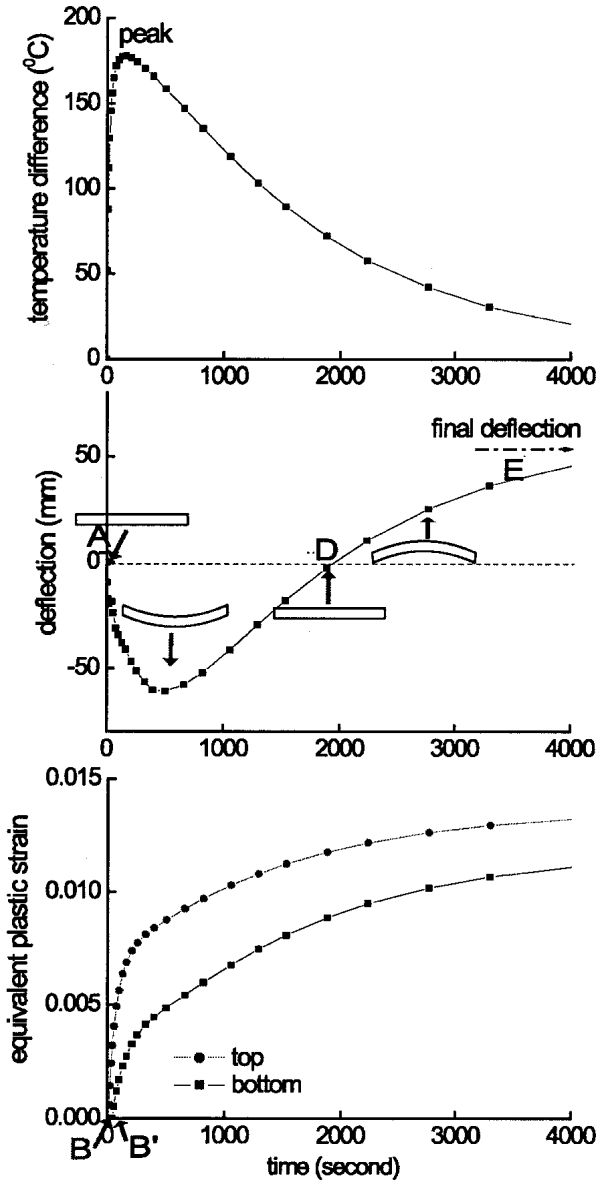

Fig. 5 Typical time-dependent temperature difference, deflection, and plastic strain under asymmetric cooling condition and inelastic behavior

loading, the largest negative (i.e., downward) deflection at center would become less negative. The deflections are always negative, maintaining positive curvature. As the yield strength of the material increases significantly, which is close to elastic case, the final deflection would approach zero.[23] Similarly, the increased thermal loading (i.e., temperature difference between top and bottom) in the current study began to induce downward deflection, which corresponded to a positive curvature (Fig. 2 and 5). As the yield strength of the slab material increases significantly, the final deflection would be close to zero (Fig. 7). Note that deflection under mechanical bending moment beyond the yield point and unloading would not display curvature reversal.[22,23] However, the reduction of the thermal loading (i.e., temperature difference) after attaining peak temperature difference may show the reversal of the curvature (Fig. 5).

Figure 8 shows a plot for the maximum deflection as ordinate and the asymmetric cooling ratio as abscissa. In the current study, the asymmetric cooling ratio was defined as the ratio between the two heat-transfer coefficients of h_1 and h_2. Unity of the asymmetric cooling ratio implies symmetric cooling condition. Under the symmetric cooling condition, top and bottom contracted identically, thus no deflection occurred even when the deformation was under inelastic region. For the coefficient h_2 between 1000 and 50 W/m^{2}K, the maximum final deflection for the slab was increased with the reduction of the coefficient h_2. Until the coefficient at bottom (h_2) was decreased from 1000 to about 50 W/m^{2}K, the heat loss at bottom through convection was sufficiently large to induce large temperature gradient and plastic strain at both top and bottom regions. The combination of thermal gradient and inelastic strains at top and bottom regions acted as a driving force for increasing the final deflection (Fig. 8). For these asymmetric cooling ratios, the highest temperature was found to occur between center and bottom (Fig. 3b).

For the coefficient h_2 was selected below 50 W/m^{2}K (for stainless steel 304), it is interesting to note that the computed final deflection was decreased with further reduction of the coefficient h_2 to 0 W/m^{2}K. If the coefficient h_2 was as low as 0 W/m^{2}K, the heat loss at bottom through convection was essentially restricted. The heat at the center region was cooled through conduction toward the top surface, leaving the highest gradient. The reduced thermal gradient at bottom generated much smaller strain gradient and smaller plastic strain at bottom than that at top. The plastic strain, which had significantly developed only at top, had lead to less final deflection compared with the situation for plastic strain developing both top and bottom. Figure 7 showed that the reduced plastic strain resulted in a reduced final deflection. Therefore, the maximum deflection for the slab could range from a very small value up to several tens of millimeters depending on the asymmetric cooling ratio inside the cooling pit. Because the computed deflection caused by the temperature difference was larger than the static deflection due to own weight inside the cooling pit, the static deflection was not included. A fictitious slab material possessing higher thermal conductivity of 50 W/mK resulted in reduced final deflection (Fig. 8) because the enhanced thermal diffusion had introduced reduced thermal gradient. The material with higher thermal conductivity compared with stainless steel can be, for example, carbon steel.[18]

As shown in Fig. 5, the sign and the magnitude of the curvature for the slab were different depending on the staying time inside the cooling pit. If the slab were withdrawn shortly after the beam was plunged into the cooling pit (i.e., between A-B in Fig. 5), the slab would not experience significant plastic deformation. The remaining and rather slow cooling in air, whether symmetric or asymmetric, would not produce significant final deflection (see Fig. 6a, b, and Fig. 9a). Second, once the slab began to experience asymmetric temperature profiles along with plastic deformation (i.e., between B-D in Fig. 5), the slab would appear to have positive curvature at the time of withdrawal from the cooling pit. During the remaining air-cooling period, the slab would continue to deform, and eventually switch the sign of the curvature due to the generated

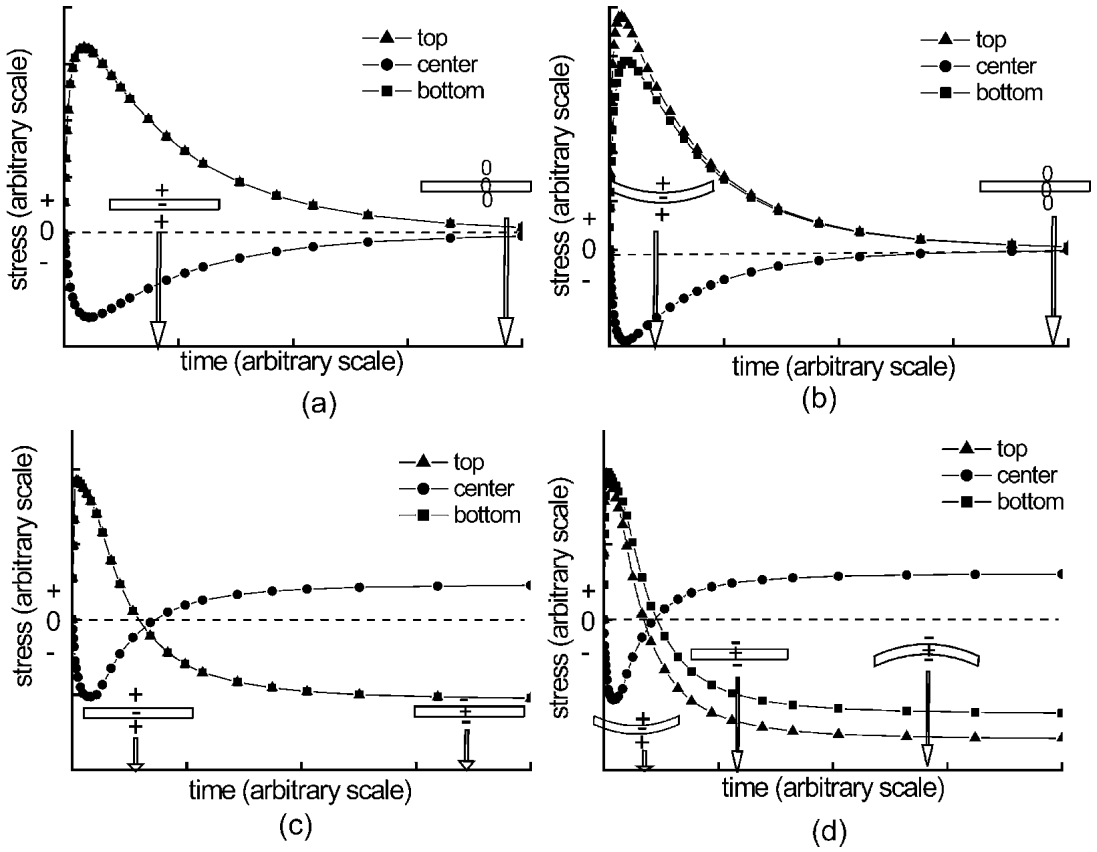

Fig. 6 Typical stress and shape changes under four different combinations: **(a)** symmetric cooling and elastic; **(b)** asymmetric cooling and elastic; **(c)** symmetric cooling and elastic-plastic; and **(d)** asymmetric cooling and elastic-plastic

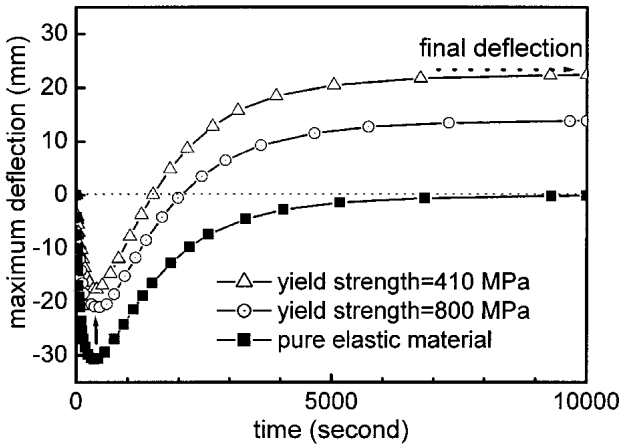

Fig. 7 Changes in time-dependent deflection depending on yield strength

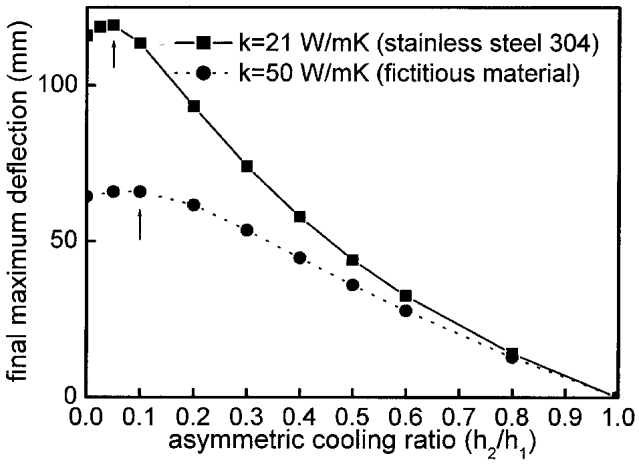

Fig. 8 Maximum final deflection depending on the asymmetric cooling ratio and the thermal conductivities

plastic strain (Fig. 9b). This type of deformation is shown in Fig. 2. Third, if the slab were left to cool for a long period (i.e., after D in Fig. 5), then the slab would readily experience the reversed curvature inside the cooling pit. The slab would exhibit and maintain a negative curvature after withdrawal from the cooling pit (Fig. 9c).

The results of this study can be used to investigate ways to control the deformation and the residual stress. In addition, the dimension of the slab material in the present work was substantially large compared with that of the material dealing with residual stress in micro-scale. However, the analysis methodology in the present work may be used to study the deformation behavior of the multi-layered materials as found in TBC (thermal barrier coating), thin solid film, or FGM (functionally

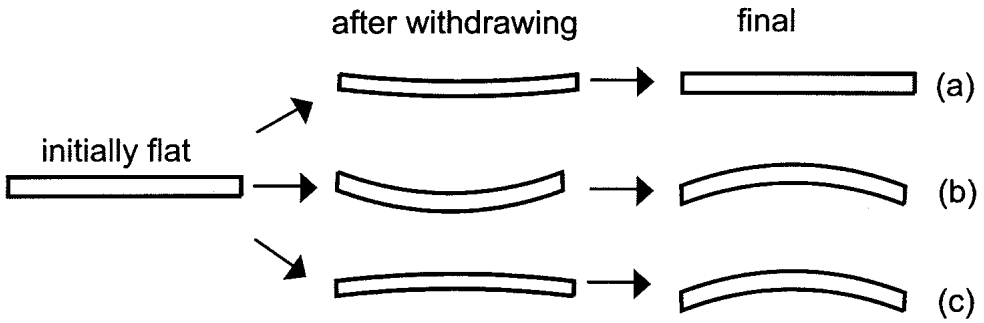

Fig. 9 Three different time-dependent deformed shapes depending on the staying time in the cooling pit: **(a)** short, **(b)** intermediate, and **(c)** prolonged period

gradient material).[24] The ceramic/metal layers with various coefficients of thermal expansion and different degree of yielding may produce different bent shapes after uniform or nonuniform temperature change. Determining the final deformed shape and residual stress for the advanced materials are reported to be crucial, because those tend to be exposed to thermal cycling causing the accumulation of plastic strains and/or oxidation-induced strains.[25] The information about final state may be used to explain the ensuing mechanical behavior for the materials.

4. Conclusions

The intrinsic transient temperature difference between surface and inner volume during rapid cooling, together with asymmetric cooling condition at the top and bottom surfaces, yielded asymmetric thermal gradient within the slab. The asymmetric cooling condition inside the cooling pit has made the flat slab begin deflecting downward immediately after being plunged into the cooing pit. The asymmetric temperatures combined with an inelastic material behavior were determined to be responsible for the time-dependent deflection accompanying a reversal of the curvature for the slab. The shape of the slab may appear different depending on the staying time inside the cooling pit, and the observed instant for the slab. The low thermal conductivity or yield strength could display an increase for the final deflection. The results explained the physical cause of the deformation reasonably well.

Acknowledgment

This work was supported by POSCO under a research grant.

References

1. J. Salsgiver and P. Maziasz: "Stainless Steels Conference 2002," *Adv. Mater. Proc.,* 2002, *160*(7), pp. 42-43.
2. J.K. Brimacombe: "The Challenge of Quality in Continuous Casting Processes," *Metall. Mater. Trans. 30B*, 1999, pp. 553-66.
3. L. Zhang, S. Taniguchi, and K. Cai: "Fluid Flow and Inclusion Removal and Continuous Casting Tundish," *Metall. Mater. Trans. 31B*(2), 2000, pp. 253-66.
4. H. Park, H. Nam, and J.K. Yoon: "Numerical Analysis of Fluid Flow and Heat Transfer in the Parallel Type Mold of a Thin Slab Caster," *ISIJ Int.,* 2001, *41*(9), pp. 974-80.
5. M. Hadji and R. Badji: "Microstructure and Mechanical Properties of Austenitic Stainless Steels After Cold Rolling," *J. Mater. Eng. Perform.,* 2002, *11*(2), pp. 145-51.
6. Y.D. Wang, R.L. Peng, X.L. Wang, and R.L. McGreevy: "Grain-orientation-dependent Residual Stress and the Effect of Annealing in Cold-Rolled Stainless Steel," *Acta Mater.*, 2002, *50,* pp. 1717-34.
7. J. Grum and R. Sturm: "Residual Stress State After the Laser Surface Remelting Process," *J. Mater. Eng. Perform.*, 2001, *10*(3), pp. 270-81.
8. D.R. Clarke: "Stress Generation During High-Temperature Oxidation of Metallic Alloys," *Curr. Opin. Solid State and Mater. Sci*., 2002, *6,* pp. 237-44.
9. H. Chang, S. Park, S. Choi, and T. Kim: "Effects of Residual Stress on Fracture Strength of Si_3N_4/Stainless Steel Joint With a Cu Interlayer," *J. Mater. Eng. Perform.*, 2002, *11*(6), pp. 640-44.
10. J. Matejicek and S. Sampath: "Intrinsic Residual Stresses in Single Splats Produced by Thermal Spray Processes," *Acta Mater.*, 2001, *49,* pp. 1993-99.
11. J. Lee, J. Mok, and C.P. Hong: "Straightforward Numerical Analysis of Casting Process in a Rectangular Mold: From Filling to Solidification," *ISIJ Int*., 1999, *39,* pp. 1252-61.
12. J. Lee, H. Han, K.H. Oh, and J.K. Yoon: "A Fully Coupled Analysis of Fluid Flow, Heat Transfer and Stress in Continuous Round Billet Casting," *ISIJ Int*., 1999, *39,* pp. 435-44.
13. S. Whitaker: *Fundamental Principles of Heat Transfer*, Krieger, 1977, pp. 477-81.
14. N.H. Pryds, J.H. Hattel, T.B. Pedersen, and J. Thorborg: "An Integrated Numerical Model of the Spray Forming Process," *Acta Mater*., 2002, *50,* pp. 4075-91.
15. J. Yanagimoto, T. Ito, and J. Liu: "FE-based Analysis for the Microstructure Evolution in Hot Bar Rolling," *ISIJ Int*., 2000, *40*(1), pp. 65-70.
16. B. Smoljan: "Numerical Simulation of Steel Quenching," *J. Mater. Eng. Perform.,* 2002, *11*(1), pp. 75-79.
17. J.M. Gere: *Mechanics of Materials*, Brooks/Cole, 2001, p. 314.
18. P.D. Harvery: *Engineering Properties of Steels*, ASM, U.S.A. 1982, pp. 273-77.
19. *ABAQUS/Standard User's Manual*, Hibbit, Kaarlson & Sorenson Inc, Providence, RI, 2002.
20. D.R. Pitts and L.E. Sissom: *Heat Transfer*, McGraw Hill, 1991, p. 87.
21. T.J. Lu and N.A. Fleck: "The Thermal Shock Resistance of Solids," *Acta Mater.*, 1998, *46,* pp. 4755-68.
22. N.E. Dowling: *Mechanical Behavior of Materials*, Prentice-Hall, 2000, pp. 613-15.
23. R. Cook and W.C. Young: *Advanced Mechanics of Materials*, Prentice-Hall, 1999, pp. 352-53.
24. S. Suresh and A. Mortensen: "Functionally Graded Metals and Metal-ceramic Composites," *Int. Mater. Rev.*, 1997, *42*(3), pp. 85-115.
25. V.K. Tolpygo and D.R. Clarke: "Tensile Cracking During Thermal Cycling of Alumina Films Formed by High-Temperature Oxidation," *Acta Mater.,* 1999, *47,* pp. 3589-605.